Qualitative behaviour and numerical approximation of solutions to conservation laws with non-local point constraints on the flux and modeling of crowd dynamics at the bottlenecks

Boris Andreianov[a], Carlotta Donadello[a], Ulrich Razafison[a,*], Massimiliano D. Rosini[b]

*[a]Laboratoire de Mathématiques, Université de Franche-Comté,
16 route de Gray, 25030 Besançon Cedex, France*
[b] ICM, University of Warsaw
ul. Prosta 69, P.O. Box 00-838, Warsaw, Poland

Abstract

In this paper we investigate numerically the model for pedestrian traffic proposed in [B. Andreianov, C. Donadello, M.D. Rosini, Crowd dynamics and conservation laws with nonlocal constraints and capacity drop, Mathematical Models and Methods in Applied Sciences 24 (13) (2014) 2685-2722] . We prove the convergence of a scheme based on a constraint finite volume method and validate it with an explicit solution obtained in the above reference. We then perform *ad hoc* simulations to qualitatively validate the model under consideration by proving its ability to reproduce typical phenomena at the bottlenecks, such as Faster Is Slower effect and the Braess' paradox.

Keywords: finite volume scheme, scalar conservation law, non-local point constraint, crowd dynamics, capacity drop, Braess' paradox, Faster Is Slower
2000 MSC: 35L65, 90B20, 65M12, 76M12

1. Introduction

Andreianov, Donadello and Rosini developed in [1] a macroscopic model, called here ADR, aiming at describing the behaviour of pedestrians at bottlenecks. The model is given by the Cauchy problem for a scalar hyperbolic conservation law in one space dimension with non-local point constraint of the form

$$\partial_t \rho + \partial_x f(\rho) = 0 \qquad\qquad (t, x) \in \mathbb{R}_+ \times \mathbb{R}, \qquad (1a)$$

$$\rho(0, x) = \bar{\rho}(x) \qquad\qquad x \in \mathbb{R}, \qquad (1b)$$

$$f\left(\rho(t, 0\pm)\right) \le p\left(\int_{\mathbb{R}_-} w(x)\, \rho(t, x)\, \mathrm{d}x\right) \qquad\qquad t \in \mathbb{R}_+, \qquad (1c)$$

where $\rho(t, x) \in [0, R]$ is the (mean) density of pedestrians in $x \in \mathbb{R}$ at time $t \in \mathbb{R}_+$ and $\bar{\rho} \colon \mathbb{R} \to [0, R]$ is the initial (mean) density, with $R > 0$ being the maximal density. Then, $f \colon [0, R] \to \mathbb{R}_+$ is the flow considered to be bell-shaped, which is an assumption commonly used in crowd dynamics. A typical example of such flow is the so-called Lighthill-Whitham-Richards (LWR) flux [2, 3, 4] defined by

$$f(\rho) = \rho\, v_{\max}\left(1 - \frac{\rho}{\rho_{\max}}\right),$$

where $v_{\max}$ and $\rho_{\max}$ are the maximal velocity and the maximal density of pedestrians respectively. Throughout this paper the LWR flux will be used. Next $p \colon \mathbb{R}_+ \to \mathbb{R}_+$ prescribes the maximal flow allowed through a bottleneck located at $x = 0$ as a function of the weighted average density in a left neighbourhood of the bottleneck and $w \colon \mathbb{R}_- \to \mathbb{R}_+$ is the weight function used to average the density.

Finally in (1c), $\rho(t, 0-)$ denotes the left measure theoretic trace along the constraint, implicitly defined by

$$\lim_{\varepsilon \downarrow 0} \frac{1}{\varepsilon} \int_0^{+\infty} \int_{-\varepsilon}^0 |\rho(t, x) - \rho(t, 0-)|\, \phi(t, x)\, \mathrm{d}x\, \mathrm{d}t = 0 \qquad\qquad \text{for all } \phi \in \mathbf{C}_{\mathbf{c}}^\infty(\mathbb{R}^2; \mathbb{R}).$$

---

*Corresponding author
Email addresses:* boris.andreianov@univ-fcomte.fr (Boris Andreianov), carlotta.donadello@univ-fcomte.fr (Carlotta Donadello), ulrich.razafison@univ-fcomte.fr (Ulrich Razafison), mrosini@icm.edu.pl (Massimiliano D. Rosini)

The right measure theoretic trace, $\rho(t, 0+)$, is defined analogously.

In the last few decades, the study of the pedestrian behaviour through bottlenecks, namely at locations with reduced capacity, such as doors, stairs or narrowings, drawn a considerable attention. The papers [5, 6, 7, 8, 9, 10, 11] present results of empirical experiments. However, for safety reasons, experiments reproducing extremal conditions such as evacuation and stampede are not available. In fact, the unique experimental study of a crowd disaster is proposed in [12]. The available data show that the capacity of the bottleneck (i.e. the maximum number of pedestrians that can flow through the bottleneck in a given time interval) can drop when high-density conditions occur upstream of the bottleneck. This phenomenon is called *capacity drop* and can lead to extremely serious consequences in escape situations. In fact, the crowd pressure before an exit can reach very high values, the efficiency of the exit dramatically reduces and accidents become more probable due to the overcrowding and the increase of the evacuation time (i.e. the temporal gap between the times in which the first and the last pedestrian pass through the bottleneck). A linked phenomenon is the so-called *Faster Is Slower* (FIS) effect, first described in [13]. FIS effect refers to the jamming and clogging at the bottlenecks, that result in an increase of the evacuation time when the degree of hurry of a crowd is high. We recall that the capacity drop and the FIS effect are both experimentally reproduced in [6, 14]. A further related (partly counter-intuitive) phenomenon is the so-called *Braess' paradox* for pedestrian flows [15]. It is well known that placing a small obstacle before an exit door can mitigate the inter-pedestrian pressure and, under particular circumstances, it reduces the evacuation time by improving the outflow of people.

Note that as it happens for any first order model, see for instance [16, Part III] and the references therein, ADR can not explain the capacity drop and collective behaviours at the bottlenecks. Therefore one of the difficulties we have to face is that the constraint p has to be deduced together with the fundamental diagram from the empirical observations.

The aim of this paper is to validate ADR by performing simulations in order to show the ability of the model to reproduce the main effects described above and related to capacity drop that are FIS and Braess' paradox. To this end we propose a numerical scheme for the model and prove its convergence. The scheme is obtained by adapting the local constrained finite volume method introduced in [17] to the non-local case considered in ADR, using a splitting strategy.

The paper is organized as follows. In Section 2 we briefly recall the main theoretical results for ADR. In Section 3 we introduce the numerical scheme, prove its convergence and validate it with an explicit solution obtained in [1]. In Section 4 we perform simulations to show that ADR is able to reproduce the Braess' paradox and the FIS effect. In Subsection 4.3 we combine local and non-local constraints to model a slow zone placed before the exit. Conclusions and perspectives are outlined in Section 5.

2. Well-posedness for the ADR model

Existence, uniqueness and stability for the general Cauchy problem (1) are established in [1] under the following assumptions:

> **(F)** f belongs to **Lip** $([0, R]; [0, +\infty[)$ and is supposed to be bell-shaped, that is $f(0) = 0 = f(R)$ and there exists $\sigma \in]0, R[$ such that $f'(\rho)(\sigma - \rho) > 0$ for a.e. $\rho \in [0, R]$.
>
> **(W)** w belongs to $\mathbf{L}^\infty(\mathbb{R}_-; \mathbb{R}_+)$, is an increasing map, $\|w\|_{\mathbf{L}^1(\mathbb{R}_-)} = 1$ and there exists $\mathrm{i}_w > 0$ such that $w(x) = 0$ for any $x \le -\mathrm{i}_w$.
>
> **(P)** p belongs to **Lip** $([0, R];]0, f(\sigma)])$ and is a non-increasing map.

The regularity $w \in \mathbf{L}^\infty(\mathbb{R}_-; \mathbb{R}_+)$ is the minimal requirement needed in order to prove existence and uniqueness of (1). In this paper, we shall consider continuous w.

The existence of solutions for the Riemann problem for (1) is proved in [18] for piecewise constant p. However, such hypothesis on p is not sufficient to ensure uniqueness of solutions, unless the flux f and the efficiency p satisfy a simple geometric condition, see [18] for details. In the present paper, we consider either continuous nonlinear p or a piecewise constant p that satisfies such geometric condition.

The definition of entropy solution for a Cauchy problem (1a), (1b) with a fixed *a priori* time dependent constraint condition

$$f(\rho(t, 0\pm)) \le q(t) \qquad\qquad t \in \mathbb{R}_+ \qquad\qquad (2)$$

was introduced in [19, Definition 3.2] and then reformulated in [17, Definition 2.1], see also [17, Proposition 2.6] and [20, Definition 2.2]. Such definitions are obtained by adding a term that accounts for the constraint in the classical definition of entropy solution given by Kruzkov in [21, Definition 1]. The definition of entropy solution given in [1, Definition 2.1] is obtained by extending these definitions to the framework of non-local constraints.

The following theorem on existence, uniqueness and stability of entropy solutions of the constrained Cauchy problem (1) is achieved under the hypotheses **(F)**, **(W)** and **(P)**.

Theorem 2.1 (Theorem 3.1 in [1]). *Let (F), (W), (P) hold. Then, for any initial datum $\bar{\rho} \in \mathbf{L}^{\infty}(\mathbb{R}; [0, R])$, the Cauchy problem (1) admits a unique entropy solution ρ. Moreover, if $\rho' = \rho'(t, x)$ is the entropy solution corresponding to the initial datum $\bar{\rho}' \in \mathbf{L}^{\infty}(\mathbb{R}; [0, R])$, then for all $T > 0$ and $L > i_w$, the following inequality holds*

$$\left\| \rho(T) - \rho'(T) \right\|_{\mathbf{L}^1([-L,L])} \le e^{CT} \left\| \bar{\rho} - \bar{\rho}' \right\|_{\mathbf{L}^1(\{|x| \le L + MT\})}, \tag{3}$$

where $M = \mathrm{Lip}(f)$ and $C = 2\mathrm{Lip}(p)\|w\|_{\mathbf{L}^{\infty}(\mathbb{R}_-)}$.

The total variation of the solution may in general increase due to the presence of the constraint. In [1] the authors provide an invariant domain $\mathcal{D} \subset \mathbf{L}^1(\mathbb{R}; [0, R])$ such that if $\bar{\rho}$ belongs to $\mathcal{D}$, then one obtains a Lipschitz estimate with respect to time of the $\mathbf{L}^1$ norm and an a priori estimate of the total variation of

$$\Psi(\rho) = \mathrm{sign}(\rho - \sigma)[f(\sigma) - f(\rho)] = \int_{\sigma}^{\rho} \left| \dot{f}(r) \right| \mathrm{d}r.$$

3. Numerical method for approximation of ADR

In this section we describe the numerical scheme based on finite volume method that we use to solve (1). Then we prove the convergence of our scheme and validate it by comparison with an explicit solution of (1). In what follows, we assume that **(F)**, **(W)** and **(P)** hold.

3.1. Non-local constrained finite volume method

Let Δx and Δt be the constant space and time steps respectively. We define the points $x_{j+1/2} = j\Delta x$, the cells $K_j = [x_{j-1/2}, x_{j+1/2}[$ and the cell centers $x_j = (j - 1/2)\Delta x$ for $j \in \mathbb{Z}$. We define the time discretization $t^n = n\Delta t$. We introduce the index j_c such that $x_{j_c+1/2}$ is the location of the constraint (a door or an obstacle). For $n \in \mathbb{N}$ and $j \in \mathbb{Z}$, we denote by ρ_j^n the approximation of the average of $\rho(t^n, \cdot)$ on the cell K_j, namely

$$\rho_j^0 = \frac{1}{\Delta x} \int_{x_{j-1/2}}^{x_{j+1/2}} \bar{\rho}(x)\,\mathrm{d}x \qquad \text{and} \qquad \rho_j^n \simeq \frac{1}{\Delta x} \int_{x_{j-1/2}}^{x_{j+1/2}} \rho(t^n, x)\,\mathrm{d}x \qquad \text{if } n > 0.$$

We recall that for the classical conservation law (1a)-(1b), a standard finite volume method can be written into the form

$$\rho_j^{n+1} = \rho_j^n - \frac{\Delta t}{\Delta x} \left(\mathcal{F}_{j+1/2}^n - \mathcal{F}_{j-1/2}^n \right), \tag{4}$$

where $\mathcal{F}_{j+1/2}^n = F\left(\rho_j^n, \rho_{j+1}^n\right)$ is a monotone, consistent numerical flux, that is, F satisfies the following assumptions:

- F is Lipschitz continuous from $[0, R]^2$ to $\mathbb{R}$ with Lipschitz constant $\mathrm{Lip}(F)$,

- $F(a, a) = f(a)$ for any $a \in [0, R]$,

- $(a, b) \in [0, R]^2 \mapsto F(a, b) \in \mathbb{R}$ is non-decreasing with respect to a and non-increasing with respect to b.

We also recall that in [17] the numerical flux for the time dependent constraint (2) is modified as follow in order to take into account the constraint condition

$$\mathcal{F}_{j+1/2}^n = \begin{cases} F\left(\rho_j^n, \rho_{j+1}^n\right) & \text{if } j \ne j_c, \\ \min\left\{ F\left(\rho_j^n, \rho_{j+1}^n\right), q^n \right\} & \text{if } j = j_c, \end{cases} \tag{5}$$

where q^n is an approximation of $q(t^n)$. In the present paper, when dealing with a Cauchy problem subject to a non-local constraint of the form (1c) we will use the approximation

$$q^n = p\left(\Delta x \sum_{j \le j_c} w(x_j) \rho_j^n \right). \tag{6}$$

Roughly speaking

- we apply the numerical scheme (4) for the problem (1a)-(1b),

- we apply the numerical scheme (4)-(5) for the problem (1a)-(1b)-(2),

- we apply the numerical scheme (4)-(5)-(6) for the problem (1).

3.2. Convergence of the scheme

Let us introduce the finite volume approximate solution ρ_Δ defined by

$$\rho_\Delta(t, x) = \rho_j^n \qquad\qquad \text{for } x \in K_j \text{ and } t \in [t^n, t^{n+1}[, \tag{7}$$

where the sequence $(\rho_j^n)_{j \in \mathbb{Z}, n \in \mathbb{N}}$ is obtained by the numerical scheme (4)-(5). Analogously, we also define the approximate constraint function

$$q_\Delta(t) = q^n \qquad\qquad \text{for } t \in [t^n, t^{n+1}[. \tag{8}$$

First, we prove a discrete stability estimate valid for any domain $Q = [0, T] \times \mathbb{R}$ with $T > 0$, for the scheme (4)-(5) applied to problem (1a)-(1b)-(2). This estimate can be seen as the equivalent, in this framework, of the stability result established in [17, Proposition 2.10].

Proposition 3.1. *Let $\overline{\rho}$ be in $\mathbf{L}^\infty(\mathbb{R}; [0, R])$ and q_Δ, $\hat{q}_\Delta$ be piecewise constant functions of the form* (8)*. If ρ_Δ and $\hat{\rho}_\Delta$ are the approximate solutions of* (1a)-(1b)-(2) *corresponding, respectively, to q_Δ and $\hat{q}_\Delta$ and constructed by applying the scheme* (4)-(5)*, then we have*

$$\|\rho_\Delta - \hat{\rho}_\Delta\|_{\mathbf{L}^1(Q)} \le 2T \|q_\Delta - \hat{q}_\Delta\|_{\mathbf{L}^1([0,T])}.$$

Proof. For notational simplicity, let $N = \lfloor T/\Delta t \rfloor$. Let us also introduce $(\tilde{\rho}_j^n)_{j \in \mathbb{Z}, n \in \mathbb{N}}$ defined by,

$$\tilde{\rho}_j^{n+1} = \rho_j^n - \frac{\Delta t}{\Delta x}\left(\tilde{\mathcal{F}}_{j+1/2}^n - \tilde{\mathcal{F}}_{j-1/2}^n\right), \quad \text{for any } j \in \mathbb{Z}, n \in \mathbb{N},$$

where $\tilde{\mathcal{F}}_{j+1/2}^n$ is defined by

$$\tilde{\mathcal{F}}_{j+1/2}^n = \begin{cases} F\left(\rho_j^n, \rho_{j+1}^n\right) & \text{if } j \ne j_c, \\ \min\left\{F\left(\rho_j^n, \rho_{j+1}^n\right), \hat{q}^n\right\} & \text{if } j = j_c. \end{cases}$$

Then using the definitions of $(\rho_j^n)_{j \in \mathbb{Z}, n \in \mathbb{N}}$ and $(\tilde{\rho}_j^n)_{j \in \mathbb{Z}, n \in \mathbb{N}}$, we have for any $n = 1, \dots, N$,

$$\rho_j^n = \tilde{\rho}_j^n \quad \text{if} \quad j \notin \{j_c, j_c + 1\}$$

and

$$\rho_{j_c}^n - \tilde{\rho}_{j_c}^n = -\frac{\Delta t}{\Delta x}\left(\min\left\{F\left(\rho_{j_c}^{n-1}, \rho_{j_c+1}^{n-1}\right), q^{n-1}\right\} + \min\left\{F\left(\rho_{j_c}^{n-1}, \rho_{j_c+1}^{n-1}\right), \hat{q}^{n-1}\right\}\right),$$

$$\rho_{j_c+1}^n - \tilde{\rho}_{j_c+1}^n = \frac{\Delta t}{\Delta x}\left(\min\left\{F\left(\rho_{j_c}^{n-1}, \rho_{j_c+1}^{n-1}\right), q^{n-1}\right\} - \min\left\{F\left(\rho_{j_c}^{n-1}, \rho_{j_c+1}^{n-1}\right), \hat{q}^{n-1}\right\}\right),$$

which implies that

$$\left|\rho_{j_c}^n - \tilde{\rho}_{j_c}^n\right| \le \frac{\Delta t}{\Delta x}\left|q^{n-1} - \hat{q}^{n-1}\right|, \qquad\qquad \left|\rho_{j_c+1}^n - \tilde{\rho}_{j_c+1}^n\right| \le \frac{\Delta t}{\Delta x}\left|q^{n-1} - \hat{q}^{n-1}\right|.$$

Therefore we deduce that, for any $n = 1, \dots, N$,

$$\sum_{j \in \mathbb{Z}} \left|\rho_j^n - \tilde{\rho}_j^n\right| \le 2\frac{\Delta t}{\Delta x}\left|q^{n-1} - \hat{q}^{n-1}\right|. \tag{9}$$

Besides, observe that the modification of the numerical flux at the interface $x_{j_c+1/2}$ introduced in (5) does not affect the monotonicity of the scheme (4)-(5) (see [17, Proposition 4.2]). Therefore, for any $n = 1, \dots, N$, we have

$$\sum_{j \in \mathbb{Z}} \left|\tilde{\rho}_j^n - \hat{\rho}_j^n\right| \le \sum_{j \in \mathbb{Z}} \left|\rho_j^{n-1} - \hat{\rho}_j^{n-1}\right|. \tag{10}$$

Hence thanks to (9) and (10), we can write

$$\sum_{j \in \mathbb{Z}} |\rho_j^1 - \hat{\rho}_j^1| \le \sum_{j \in \mathbb{Z}} |\rho_j^1 - \tilde{\rho}_j^1| + \sum_{j \in \mathbb{Z}} |\tilde{\rho}_j^1 - \hat{\rho}_j^1| \le 2\frac{\Delta t}{\Delta x}\left|q^0 - \hat{q}^0\right| + \sum_{j \in \mathbb{Z}} |\rho_j^0 - \hat{\rho}_j^0| = 2\frac{\Delta t}{\Delta x}\left|q^0 - \hat{q}^0\right|.$$

Then an induction argument shows that for any $n = 1, \dots, N$,

$$\sum_{j \in \mathbb{Z}} \left|\rho_j^n - \hat{\rho}_j^n\right| \le 2\frac{\Delta t}{\Delta x}\sum_{k=0}^{n-1} |q^k - \hat{q}^k| \le \frac{2}{\Delta x} \|q_\Delta - \hat{q}_\Delta\|_{L^1([0,t^n])}.$$

4

In conclusion, we find that

$$\|\rho_\Delta - \hat{\rho}_\Delta\|_{L^1(Q)} = \Delta t\,\Delta x \sum_{n=1}^{N}\sum_{j\in\mathbb{Z}} |\rho_j^n - \hat{\rho}_j^n| \leq 2\|q_\Delta - \hat{q}_\Delta\|_{L^1([0,T])} \sum_{n=1}^{N}\Delta t \leq 2T\|q_\Delta - \hat{q}_\Delta\|_{L^1([0,T])}$$

and this ends the proof. $\qquad\square$

Let us now notice that as in [17, Proposition 4.2], under the CFL condition

$$\text{Lip}(F)\,\frac{\Delta t}{\Delta x} \leq \frac{1}{2}, \tag{11}$$

we have the $\mathbf{L}^\infty$ stability of the scheme (4)-(5)-(6) that is

$$0 \leq \rho_\Delta(t,x) \leq R \qquad\qquad \text{for a.e. } (t,x) \in Q. \tag{12}$$

This stability result allows to prove the statement below.

Proposition 3.2. *Let q_Δ be defined by* (6)-(8). *Then under the CFL condition* (11), *for any $T > 0$, there exists $C > 0$ only depending on T, f, F, p, w and R such that:*

$$|q_\Delta|_{BV([0,T])} \leq C. \tag{13}$$

Proof. Let $N = \lfloor T/\Delta t \rfloor$ and j_w be an integer such that $\text{supp}(w) \subset \underset{j_w \leq j \leq j_c}{\cup} K_j$. Then for any $n = 0,\dots,N-1$, we have

$$\left|q^{n+1} - q^n\right| = \left|p\left(\Delta x \sum_{j_w \leq j \leq j_c} w(x_j)\rho_j^{n+1}\right) - p\left(\Delta x \sum_{j_w \leq j \leq j_c} w(x_j)\rho_j^{n}\right)\right|$$

$$\leq \Delta x\,\text{Lip}(p)\left|\sum_{j_w \leq j \leq j_c} w(x_j)(\rho_j^{n+1} - \rho_j^n)\right| = \Delta t\,\text{Lip}(p)\left|\sum_{j_w \leq j \leq j_c} w(x_j)\left(\mathcal{F}_{j+1/2}^n - \mathcal{F}_{j-1/2}^n\right)\right|.$$

Now, using a summation by part, we have

$$\sum_{j_w \leq j \leq j_c} w(x_j)\left(\mathcal{F}_{j+1/2}^n - \mathcal{F}_{j-1/2}^n\right) = w(x_{j_c})\mathcal{F}_{j_c+1/2}^n - w(x_{j_w})\mathcal{F}_{j_w-1/2}^n - \sum_{j_w \leq j \leq j_c-1}\left(w(x_{j+1}) - w(x_j)\right)\mathcal{F}_{j+1/2}^n.$$

Then, it follows that

$$|q^{n+1} - q^n| \leq \Delta t\,\text{Lip}(p)\,\|w\|_{\mathbf{L}^\infty(\mathbb{R}_-;\mathbb{R})} \sum_{j_w-1 \leq j \leq j_c} |\mathcal{F}_{j+1/2}^n|.$$

Now, from (5), for any $j \in \mathbb{Z}$ we have the estimate

$$\left|\mathcal{F}_{j+1/2}^n\right| \leq \left|F(\rho_j^n, \rho_{j+1}^n)\right| \leq \left|F(\rho_j^n, \rho_{j+1}^n) - F(\rho_j^n, \rho_j^n)\right| + \left|f(\rho_j^n)\right| \leq \text{Lip}(F)\left|\rho_{j+1}^n - \rho_j^n\right| + \text{Lip}(f)\left|\rho_j^n\right| \leq R\left(\text{Lip}(F) + \text{Lip}(f)\right).$$

Hence we deduce that

$$|q_\Delta|_{BV([0,T])} = \sum_{n=0}^{N-1}\left|q^{n+1} - q^n\right| \leq C,$$

where $C = (j_c - j_w + 2)\,T\,R\,\text{Lip}(p)\,\|w\|_{\mathbf{L}^\infty(\mathbb{R}_-;\mathbb{R})}\left(\text{Lip}(F) + \text{Lip}(f)\right).$ $\qquad\square$

We are now in a position to prove a convergence result for the scheme (4)-(5)-(6).

Theorem 3.1. *Under the CFL condition* (11), *the constrainted finite volume scheme* (4)-(5)-(6) *converges in $\mathbf{L}^1(Q)$ to the unique entropy solution to* (1).

Proof. Let (ρ_Δ, q_Δ) be constructed by the scheme (4)-(5)-(6). Proposition 3.2 and Helly's lemma give the existence of a subsequence, still denoted q_Δ and a constraint function $q \in \mathbf{L}^\infty([0,T])$ such that q_Δ converges to q strongly in $\mathbf{L}^1([0,T])$ as $\Delta t \to 0$. Let $\rho \in \mathbf{L}^\infty(\mathbb{R}_+ \times \mathbb{R}; [0,R])$ be the unique entropy solution to (1a)-(1b)-(2) associated to q. It remains to prove that the subsequence ρ_Δ converges to ρ strongly in $\mathbf{L}^1(Q)$ as Δt, $\Delta x \to 0$. The uniqueness of the entropy solution to (1a)-(1b)-(2) will then imply that the full sequence ρ_Δ converges to ρ and, as a consequence, the full sequence q_Δ converges to $q = p\left(\int_{\mathbb{R}_-} w(x)\rho(t,x)\,\mathrm{d}x\right)$.

Let $\hat{q}_\Delta$ be a piecewise constant approximation of q such that $\hat{q}_\Delta$ converges to q strongly in $\mathbf{L}^1([0,T])$. Furthermore, we also introduce $\hat{\rho}_\Delta$ constructed by the scheme (4)-(5) and associated to $\hat{q}_\Delta$. Now we have

$$\|\rho - \rho_\Delta\|_{\mathbf{L}^1(Q)} \leq \|\rho - \hat{\rho}_\Delta\|_{\mathbf{L}^1(Q)} + \|\rho_\Delta - \hat{\rho}_\Delta\|_{\mathbf{L}^1(Q)}.$$

But, thanks to [17, Theorem 4.9], under the CFL condition (11), $\|\rho - \hat{\rho}_\Delta\|_{\mathbf{L}^1(Q)}$ tends to 0 as Δt, $\Delta x \to 0$. Furthermore, thanks to Proposition 3.1, we have

$$\|\rho_\Delta - \hat{\rho}_\Delta\|_{\mathbf{L}^1(Q)} \leq 2\,T\,\|q_\Delta - \hat{q}_\Delta\|_{\mathbf{L}^1([0,T])}$$

which also shows that $\|\rho_\Delta - \hat{\rho}_\Delta\|_{\mathbf{L}^1(Q)}$ tends to 0 as Δt, $\Delta x \to 0$. $\qquad\square$
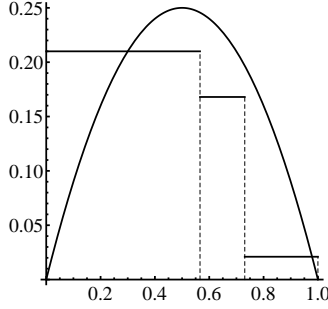
5

3.3. Validation of the numerical scheme

Figure 1: The functions $[\rho \mapsto f(\rho)]$ and $[\xi \mapsto p(\xi)]$ as in Section 3.3.

We propose here to validate the numerical scheme (4)-(5)-(6) using the Godounov numerical flux (see e.g. [22, 23]) which will be used in the remaining of this paper:

$$F(a,b) = \begin{cases} \min_{[a,b]} f & \text{if } a \le b, \\ \max_{[b,a]} f & \text{if } a > b. \end{cases}$$

We consider the explicit solution to (1) constructed in [1, Section 6] by applying the wave front tracking algorithm. The set up for the simulation is as follows. Consider the domain of computation $[-6, 1]$, take a normalized flux $f(\rho) = \rho(1-\rho)$ (namely the maximal velocity and the maximal density are assumed to be equal to one) and a linear weight function $w(x) = 2(1 + x)\chi_{[-1,0]}(x)$. Assume a uniform distribution of maximal density in $[x_A, x_B]$ at time $t = 0$, namely $\bar{\rho} = \chi_{[x_A, x_B]}$. The efficiency of the exit, p, see Figure 1, is of the form

$$p(\xi) = \begin{cases} p_0 & \text{if } 0 \le \xi < \xi_1, \\ p_1 & \text{if } \xi_1 \le \xi < \xi_2, \\ p_2 & \text{if } \xi_2 \le \xi \le 1. \end{cases}$$

The explicit solution ρ corresponding to the values

$$p_0 = 0.21, \qquad p_1 = 0.168, \qquad p_2 = 0.021, \qquad \xi_1 \sim 0.566, \qquad x_A = -5.75, \qquad x_B = -2, \qquad \xi_2 \sim 0.731,$$

is represented in Figure 2. The above choices for the flux f and the efficiency p ensure that the solution to each Riemann problem is unique, see [18]. We defer to [1, Section 6] for the details of the construction of the solution ρ and its physical interpretation.

A qualitative comparison between the numerically computed solution $x \mapsto \rho_\Delta(t, x)$ and the explicitly computed solution $x \mapsto \rho(t, x)$ at different fixed times t is in Figure 3. We observe good agreements between $x \mapsto \rho(t, x)$ and $x \mapsto \rho_\Delta(t, x)$. The parameters for the numerically computed solution are $\Delta x = 3.5 \times 10^{-4}$ and $\Delta t = 7 \times 10^{-5}$.

A convergence analysis is also performed for this test. We introduce the relative $\mathbf{L}^1$-error for the density ρ, at a given time t^n, defined by

$$E_{\mathbf{L}^1}^n = \left[\sum_j \left| \rho(t^n, x_j) - \rho_j^n \right| \right] / \left[\sum_j \left| \rho(t^n, x_j) \right| \right].$$

In Table 1, we computed the relative $\mathbf{L}^1$-errors for different numbers of space cells at the fixed time $t = 10$. We deduce that the order of convergence is approximatively 0.906. As in [17], we observe that the modification (5) of the numerical flux does not affect the accuracy of the scheme.

4. Numerical simulations

This section is devoted to the phenomenological description of some collective effects in crowd dynamics related to capacity drop, namely the Braess' paradox and the Faster Is Slower (FIS) effect.

4.1. Faster is Slower effect

The FIS effect was first described in [13, 24] in the context of the room evacuation problem. The authors studied the evolution of the evacuation time as a function of the maximal velocity reached by the pedestrians, and they shown that there exists an optimal velocity for which the evacuation time attains a minimum. Therefore, any acceleration beyond the
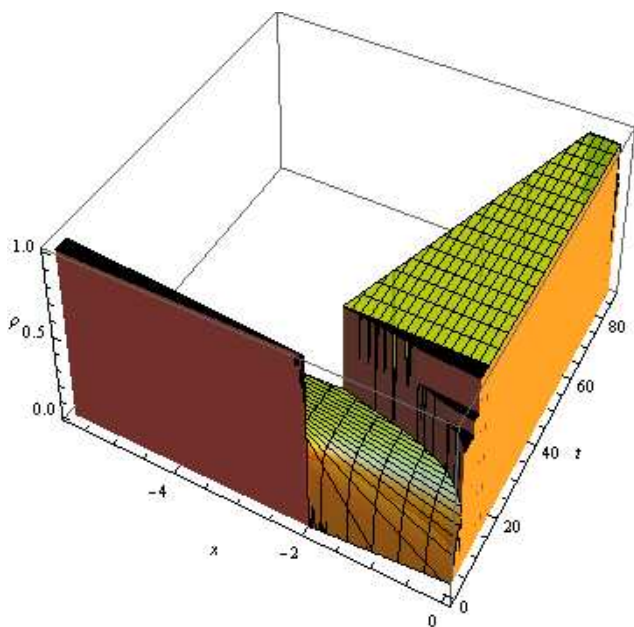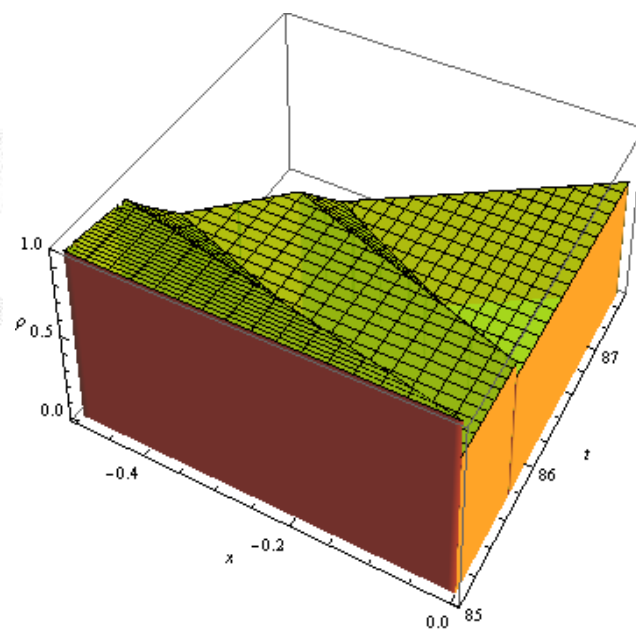
(a) The solution in the (t, x, ρ)-coordinates.
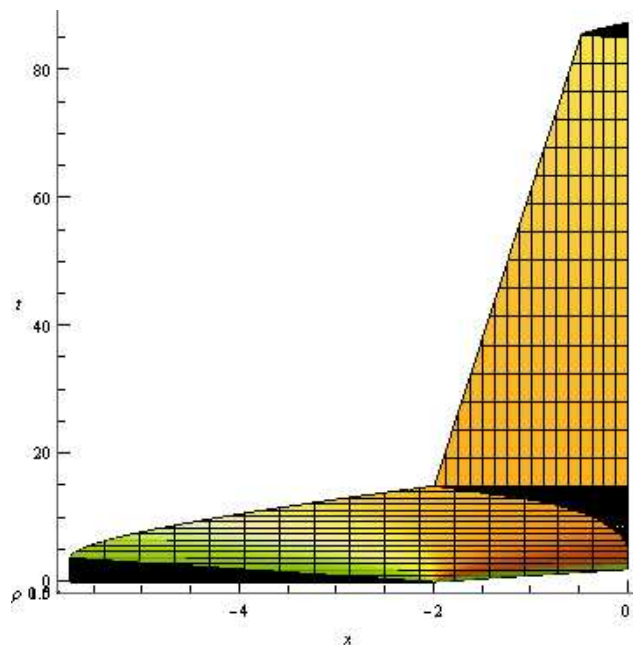
(b) The solution in the (x, t)-coordinates.
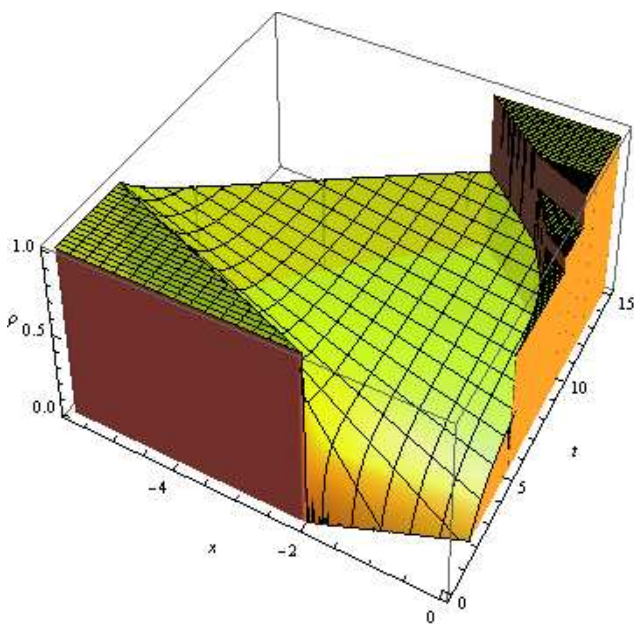
(c) The solution in the (t, x, ρ)-coordinates for $0 \leq t \leq 15$.

(d) The solution in the (t, x, ρ)-coordinates for $85 \leq t \leq 87.5$.

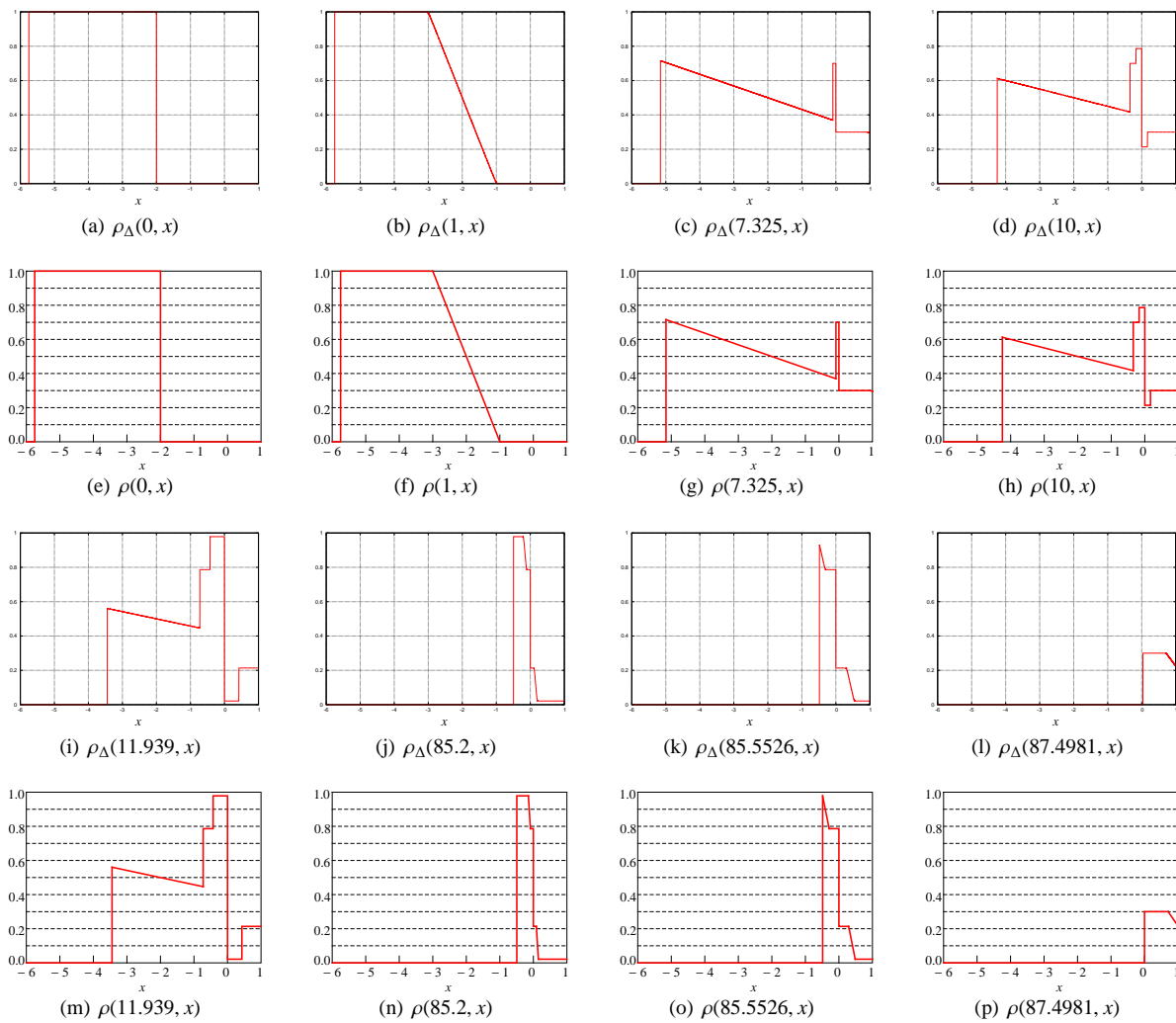Figure 2: Representation of the solution constructed in [1, Section 6] and described in Subsection 3.3.

7

Figure 3: With reference to Subsection 3.3: The numerically computed solution $x \mapsto \rho_\Delta(t, x)$ and the explicitly computed solution $x \mapsto \rho(t, x)$ at different fixed times t.

8

Number of cells	$\mathbf{L^1}$-error
625	9.6843×10^{-3}
1250	6.2514×10^{-3}
2500	3.4143×10^{-3}
5000	1.3172×10^{-3}
10000	1.03×10^{-3}
20000	4.2544×10^{-4}
Order	0.906

Table 1: Relative $\mathbf{L^1}$-error at time $t = 10$.

optimal velocity worses the evacuation time. Following the studies above, the curve representing the evacuation time as a function of the average velocity takes a characteristic shape [24, Figure 1c].

The first numerical tests we performed aim to verify if such shape is obtained starting from the ADR model. To this end, we consider the corridor modeled by the segment [-6,1], with an exit at $x = 0$. We consider the flux $f(\rho) = \rho \, v_{\max} (1 - \rho)$ where $v_{\max}$ is the maximal velocity of the pedestrians and the maximal density is equal to one. We use the same weight function as for the validation of the scheme, $w(x) = 2(1 + x)\chi_{[-1,0]}(x)$ and, the same initial density, $\bar{\rho} = \chi_{[-5.75,-2]}$. The efficiency of the exit p is now given by the following continuous function

$$
p(\xi) \quad = \begin{cases} p_0 & \text{if } 0 \leq \xi < \xi_1, \\[2mm] \dfrac{(p_0 - p_1)\xi + p_1\xi_1 - p_0\xi_2}{\xi_1 - \xi_2} & \text{if } \xi_1 \leq \xi < \xi_2, \\[2mm] p_1 & \text{if } \xi_2 \leq \xi \leq 1, \end{cases} \tag{14}
$$

where

$$ p_0 = 0.24, \qquad p_1 = 0.05, \qquad \xi_1 = 0.5, \qquad \xi_2 = 0.9. $$

The space and time steps are fixed to $\Delta x = 5 \times 10^{-3}$ and $\Delta t = 5 \times 10^{-4}$. In Figure 4 are plotted the flux f corresponding to the maximal velocity $v_{\max} = 1$ and the above efficiency of the exit.
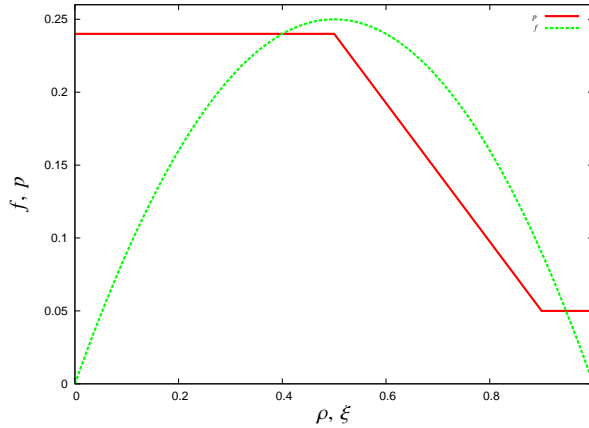

Figure 4: The normalized flux $\rho \to f(\rho)$ and the constraint $\xi \to p(\xi)$ defined in (14).

Figure 5 represents the evacuation time as a function of the maximal velocity $v_{\max}$, as $v_{\max}$ varies in the interval $[0.1, 5]$. As we can observe, the general shape described above is recovered. The numerical minimal evacuation time is 19.007 and is obtained for $v_{\max} = 1$.

In addition, we reported in Figure 6 the density at the exit as a function of time for different values of the maximal velocity $v_{\max}$ around the optimal one. We notice that the maximal density at the exit and the time length where the density is maximal increase with the velocity. This expresses the jamming at the exit that leads to the FIS effect.

Then we performed some series of tests to see how the general shape obtained in Figure 5 changes with respect to variations of the parameters of the model. In Figure 8 (a), we show this variation when we consider different initial densities, namely, $\bar{\rho}, \bar{\rho}_1$ and $\bar{\rho}_2$ with $\bar{\rho}_1(x) = 0.8\chi_{[-5.75,-2]}$ and $\bar{\rho}_2(x) = 0.6\chi_{[-5.75,-2]}$. The general shape of the curves is conserved. We observe that the evacuation time increases with the initial amount of pedestrians while the optimal velocity
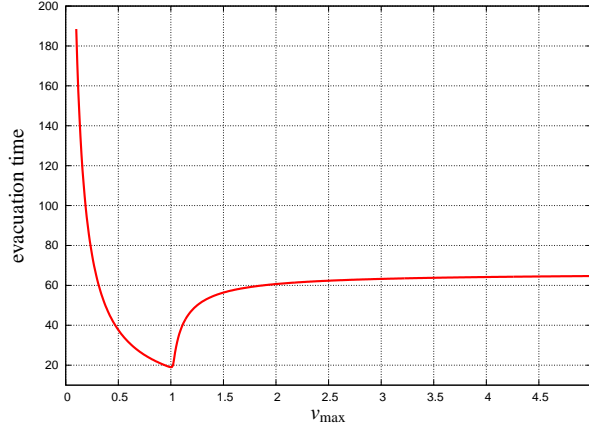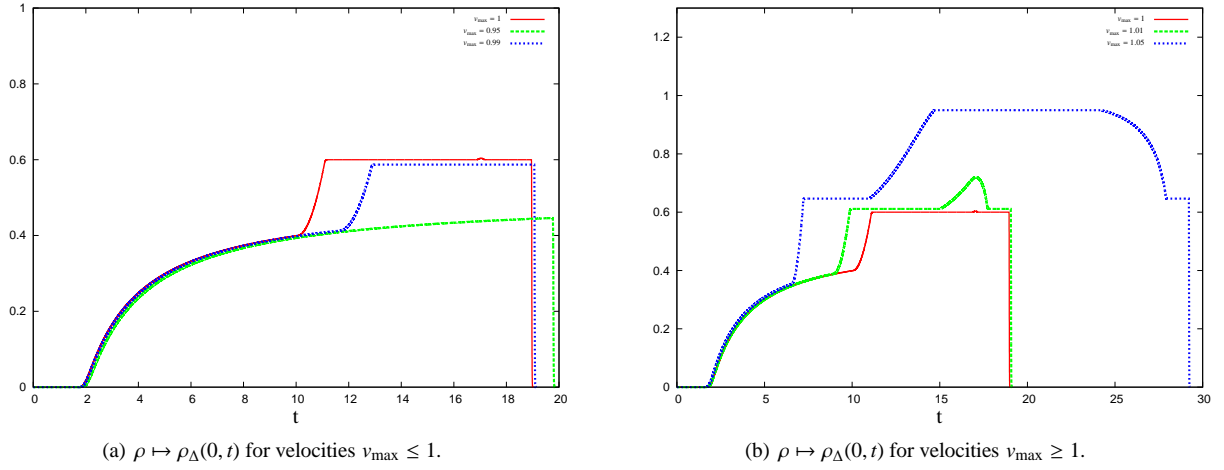
9

Figure 5: With reference to Subsection 4.1: Evacuation time as a function of the velocity $v_{\max}$.

(a) $\rho \mapsto \rho_\Delta(0, t)$ for velocities $v_{\max} \le 1$.

(b) $\rho \mapsto \rho_\Delta(0, t)$ for velocities $v_{\max} \ge 1$.

Figure 6: With reference to Subsection 4.1: Densities at the exit as a function of time for different velocities.

decreases as the initial amount of pedestrians increases. The minimal evacuation time and the corresponding optimal maximal velocity are 12.259 and 1.07 for $\bar{\rho}_2$ and 15.691 and 1.03 for $\bar{\rho}_1$.

Next we explore the case where the efficiency of the exit varies. We consider the function p defined in (14) and the modification p_β such that $p_\beta(\xi) = p(\beta\xi)$. In Figure 7, we plotted the functions p, p_β for $\beta = 0.8$ and $\beta = 0.9$. Then, in Figure 8 (b) are plotted the evacuation time curves corresponding to these three efficiencies of the exit. As minimum evacuation times, we obtain 18.586 and 18.827 for $\beta = 0.8, 0.9$ respectively. As expected, the minimal evacuation time increases with lower efficiency of the exit. The corresponding velocities are approximatively 1.06 and 1.02 respectively.

Finally, we change the location of the initial density. In addition to the corridor $[-6, 1]$, we consider two other corridors modeled by the segments $[-12, 1]$ and $[-20, 1]$. In these two corridors we take as initial densities $\bar{\rho}_3(x) = \chi_{[-11.75, -8]}$ and $\bar{\rho}_4(x) = \chi_{[-19.75, -16]}$ respectively. We have reported the obtained evacuation time curves in Figure 8 (c). As expected, the minimal evacuation time increases with the distance between the exit and the initial density location.

4.2. Braess' paradox

The presence of obstacles, such as columns upstream from the exit, may prevent the crowd density from reaching dangerous values and may actually help to minimize the evacuation time, since in a moderate density regime the full capacity of the exit can be exploited. From a microscopic point of view, the decrease of the evacuation time may seem unexpected, as some of the pedestrians are forced to chose a longer path to reach the exit.

The ADR model is able to reproduce the Braess' paradox for pedestrians, as we show in the following simulations. We consider, as in the previous subsection, the corridor modeled by the segment $[-6, 1]$ with an exit at $x = 0$. We compute the solution corresponding to the flux $f(\rho) = \rho(1 - \rho)$, the initial density $\bar{\rho}(x) = \chi_{[-5.75, -2]}(x)$, the efficiency of the exit p of the form (14) with the parameters

$$p_0 = 0.21, \qquad p_1 = 0.1, \qquad \xi_1 = 0.566, \qquad \xi_2 = 0.731$$

10
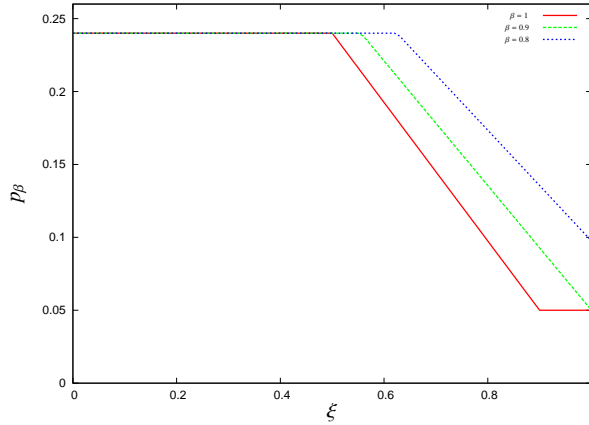
Figure 7: With reference to Subsection 4.1: The efficiencies $\xi \to p_\beta(\xi)$ for $\beta = 0.8, 0.9, 1$.

and the same weight function $w(x) = 2(1 + x)\chi_{[-1,0]}(x)$. The space and time steps are fixed to $\Delta x = 5 \times 10^{-3}$ and $\Delta t = 5 \times 10^{-4}$. Without any obstacle, the numerical evacuation time is 29.496. In these following simulations we place an obstacle at $x = d$, with $-2 < d < 0$. The obstacle reduces the capacity of the corridor and can be seen as a door, which we assume larger than the one at $x = 0$. Following these ideas we define an efficiency function $p_d(\xi) = 1.15p(\xi)$ and a weight function $w_d(x) = 2(x - d + 1)\chi_{[d-1,d]}(x)$ associated to the obstacle.

In Figure 9 we have reported the evolution of the evacuation time when the position of the obstacle varies in the interval $[-1.9, -0.01]$ with a step of 0.01. We observe that for $-1.8 \le d \le -1.72$, the evacuation time is lower than in the absence of the obstacle. The optimal position of the obstacle is obtained for $d = -1.72$ and the corresponding evacuation time is 24.246. We compare in Figure 10 five snapshots of the solution without obstacle and the solutions with an obstacle placed at $d = -1.72$ and $d = -1.85$. This latter location corresponds to a case where the evacuation time is greater than the one without an obstacle. In these snapshots, we see that the obstacle placed at $d = -1.85$ becomes congested very soon. This is due to the fact that the obstacle is too close to the location of the initial density. When the obstacle is placed at $d = -1.72$, it delays the congestion at the exit.

4.3. Zone of low velocity

In this section, we perform a series of simulations where the obstacle introduced in Subsection 4.2 is now replaced by a zone where the velocity of pedestrians is lower than elsewhere in the domain. The effect we want to observe here is similar to the one we see in Braess' Paradox. Namely we prevent an high concentration of pedestrians in front of the exit by constraining their flow in an upstream portion of the corridor. In this case however the constraint is local, as the maximal value allowed for the flow only depends on the position in the corridor.

We consider again the corridor modeled by the segment $[-6, 1]$ with an exit at $x = 0$. The efficiency of the exit and the initial density are the same as in the previous subsection. Assume that the slow zone is of size one and is centred at $x = d$, where $-1.9 \le d \le 0$. Define the following function

$$
k(x) \quad = \quad \begin{cases} 1 & \text{if } x \le d - 0.5, \\ -2(x - d) & \text{if } d - 0.5 \le x \le d, \\ 2(x - d) & \text{if } d \le x \le d + 0.5, \\ 1 & \text{if } x \ge d + 0.5, \end{cases} \tag{15}
$$

and the following velocity $v(x, \rho) = [\lambda + (1 - \lambda)\,k(x)]\,v_{max}\,(1 - \rho)$, where $\lambda \in [0, 1]$ and $v_{max} \ge 1$ is the maximal velocity. With such velocity, the maximal velocity of pedestrians decreases in the interval $[d - 0.5, d]$, reaching its minimal value $\lambda\,v_{max}$ at $x = d$. Then the velocity increases in the interval $[d, d + 0.5]$ reaching the maximum value v_{max}, that corresponds to the maximal velocity away from the slow zone. Finally we consider the flux $f(x, \rho) = \rho\,v(x, \rho)$ and the space and time steps are fixed to $\Delta x = 5 \times 10^{-3}$ and $\Delta t = 5 \times 10^{-4}$.

Figure 11 (a) shows the evolution of the evacuation time as a function of the parameter λ varying in the interval $[0.1, 1]$ when the center of the slow zone is fixed at $d = -1.5$. We observe that the optimal minimal velocity in the slow zone is for $\lambda = 0.88$ and the corresponding evacuation time is 20.945. Recalling that without the slow zone the evacuation time is 29.496, we see that the introduction of the slow zone allows to reduce the evacuation time. In Figure 11 (b), we show the evolution of the evacuation time when varying the center of the slow zone d in the interval $[-1.9, 0]$ and when the minimal

11
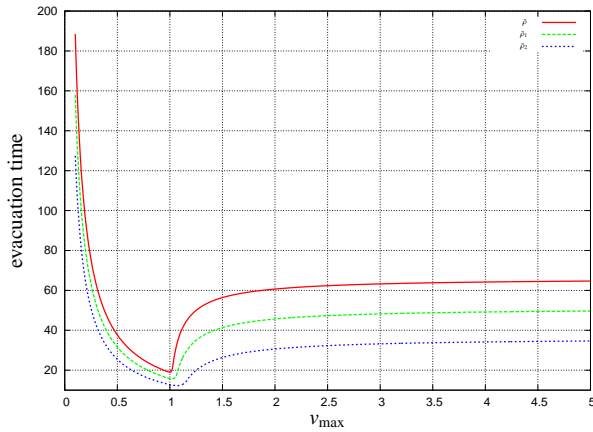
(a) Evacuation time as a function of $v_{\max}$ for different amounts of initial densities.
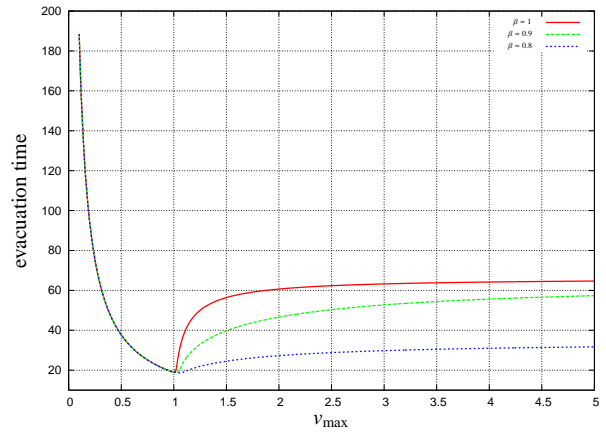
(b) Evacuation time as a function of $v_{\max}$ for different efficiencies of the exit.
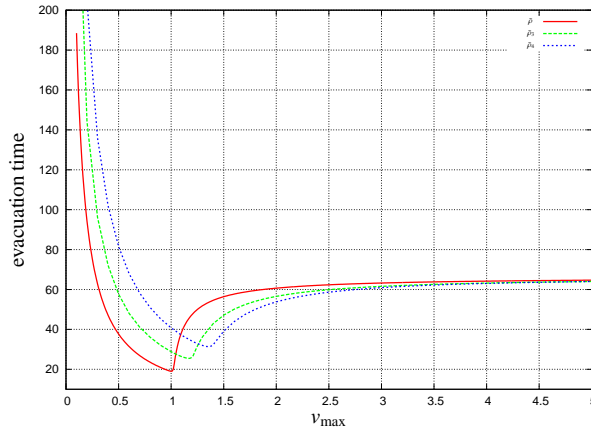
(c) Evacuation time as a function of $v_{\max}$ for different locations of the initial density.

Figure 8: With reference to Subsection 4.1: Evacuation time as a function of $v_{\max}$ for different parameters of the model.

and the maximal velocities are fixed and correspond to $\lambda = 0.88$ and $v_{\max} = 1$. We observe here that, unlike in the Braess paradox tests case, the evacuation time does not depend on the location of the slow zone, except when this latter is close enough to the exit. Indeed, when the slow zone gets too close to the exit, the evacuation time grows. This is due to the fact that pedestrians do not have time to speed up before reaching the exit.

Fix now $d = -1.5$ and $\lambda = 0.88$ and assume that $v_{\max}$ varies in the interval $[0.1, 5]$. The evolution of the evacuation time as a function of $v_{\max}$ is reported in Figure 11 (c). We observe that we get the characteristic shape already obtained in the FIS effect.

Finally we present in Figure 12 five snapshots for three different solutions. The first two solutions are the ones computed in Subsection 4.2, without obstacle and with an obstacle located at $d = -1.72$ respectively. The third solution is computed with a zone of low velocity centered at $d = -1.72$, $\lambda = 0.88$ and $v_{\max} = 1$. In order to have a good resolution of this third solution, the space and time steps where fixed to $\Delta x = 3.5 \times 10^{-4}$ and $\Delta t = 7 \times 10^{-5}$. We note that in the case where a zone of low velocity is placed in the domain, we do not see the capacity drop, as the density of pedestrians never attains very high values in the region next to the exit.

5. Conclusions

Qualitative features that are characteristic of pedestrians' macroscopic behaviour at bottlenecks (Faster is Slower, Braess' paradox) are reproduced in the setting of the simple scalar model with non-local point constraint introduced in [1]. These effects are shown to be persistent for large intervals of values of parameters. The validation is done by means of a simple and robust time-explicit splitting finite volume scheme which is proved to be convergent, with experimental rate close to one.

The results presented in this paper allow to consider more complex models. Indeed, as ADR is a first order model, it is not able to capture more complicated effects related to crowd dynamics. Typically, ADR fails to reproduce the
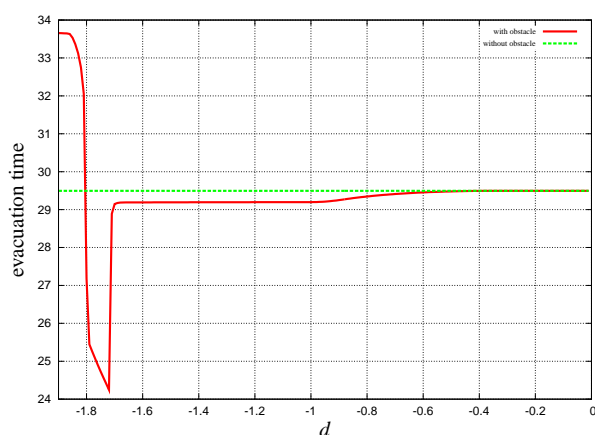
Figure 9: With reference to Subsection 4.2: Evacuation time as a function of the position of the obstacle.

amplification of small perturbations. This leads to consider second order model such as the model proposed by Aw, Rascle and Zhang [25, 26] in the framework of vehicular traffic.

Another extension of this work is to consider the ADR model with constraints that are non-local in time. Such constraints allow to tackle optimal management problems in the spirit of [27, 28].

Finally, this work can also be extended to two-dimensional models where experimental validations may be possible.

Acknowledgment

References

[1] B. Andreianov, C. Donadello, M. D. Rosini, Crowd dynamics and conservation laws with nonlocal constraints and capacity drop, Mathematical Models and Methods in Applied Sciences 24 (13) (2014) 2685–2722. doi:10.1142/S0218202514500341.

[2] M. J. Lighthill, G. B. Whitham, On Kinematic Waves. II. A Theory of Traffic Flow on Long Crowded Roads, Royal Society of London Proceedings Series A 229 (1955) 317–345. doi:10.1098/rspa.1955.0089.

[3] P. I. Richards, Shock waves on the highway, Operations Research 4 (1) (1956) 42–51. doi:10.1287/opre.4.1.42.

[4] B. D. Greenshields, A study of traffic capacity, Proceeding of the Highway Research Board 14 (1934) 448–477.

[5] A. Schadschneider, W. Klingsch, H. Klüpfel, T. Kretz, C. Rogsch, A. Seyfried, Evacuation Dynamics: Empirical Results, Modeling and Applications, in: R. A. Meyers (Ed.), Extreme Environmental Events, Springer New York, 2011, pp. 517–550. doi:10.1007/978-1-4419-7695-6_29.

[6] E. M. Cepolina, Phased evacuation: An optimisation model which takes into account the capacity drop phenomenon in pedestrian flows, Fire Safety Journal 44 (4) (2009) 532–544. doi:10.1016/j.firesaf.2008.11.002.

[7] S. P. Hoogendoorn, W. Daamen, Pedestrian behavior at bottlenecks, Transportation Science 39 (2) (2005) 147–159. doi:10.1287/trsc.1040.0102.

[8] V. Kopylow, The study of people' motion parameters under forced egress situations, Ph.D. Thesis, Moscow Civil Engineering Institute (1974).

[9] T. Kretz, A. Grünebohm, M. Kaufman, F. Mazur, M. Schreckenberg, Experimental study of pedestrian counterflow in a corridor, Journal of Statistical Mechanics: Theory and Experiment 2006 (10) (2006) P10001. doi:10.1088/1742-5468/2006/10/P10001.

[10] A. Seyfried, T. Rupprecht, A. Winkens, O. Passon, B. Steffen, W. Klingsch, M. Boltes, Capacity Estimation for Emergency Exits and Bottlenecks, in: Interflam 2007, 2007, pp. 247–258, record converted from VDB: 12.11.2012. URL http://juser.fz-juelich.de/record/59568

[11] X. L. Zhang, W. G. Weng, H. Y. Yuan, J. G. Chen, Empirical study of a unidirectional dense crowd during a real mass event, Physica A: Statistical Mechanics and its Applications 392 (12) (2013) 2781–2791.

[12] D. Helbing, A. Johansson, H. Z. Al-Abideen, Dynamics of crowd disasters: An empirical study, Phys. Rev. E 75 (2007) 046109. doi:10.1103/PhysRevE.75.046109.

[13] D. Helbing, I. Farkas, T. Vicsek, Simulating dynamical features of escape panic, Nature 407 (6803) (2000) 487–490. doi:doi:10.1038/35035023.

[14] S. A. Soria, R. Josens, D. R. Parisi, Experimental evidence of the "Faster is Slower" effect in the evacuation of ants, Safety Science 50 (7) (2012) 1584–1588. doi:10.1016/j.ssci.2012.03.010.

[15] R. L. Hughes, The flow of human crowds, Annual review of fluid mechanics 35 (1) (2003) 169–182. doi:10.1146/annurev.fluid.35.101101.161136.

[16] M. D. Rosini, Macroscopic models for vehicular flows and crowd dynamics: theory and applications, Understanding Complex Systems, Springer, Heidelberg, 2013. doi:10.1007/978-3-319-00155-5. URL http://dx.doi.org/10.1007/978-3-319-00155-5

[17] B. Andreianov, P. Goatin, N. Seguin, Finite volume schemes for locally constrained conservation laws, Numerische Mathematik 115 (2010) 609–645. doi:10.1007/s00211-009-0286-7.
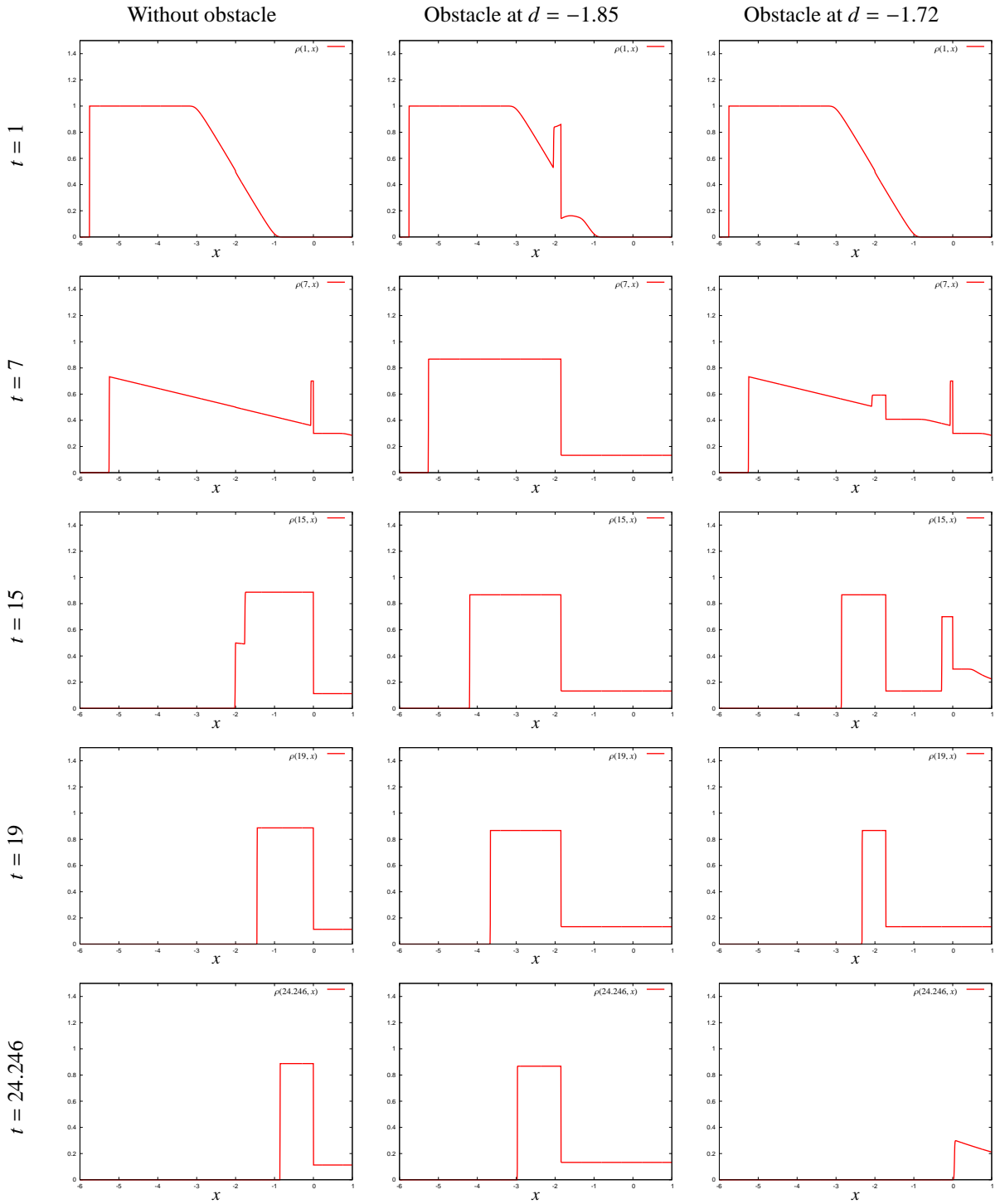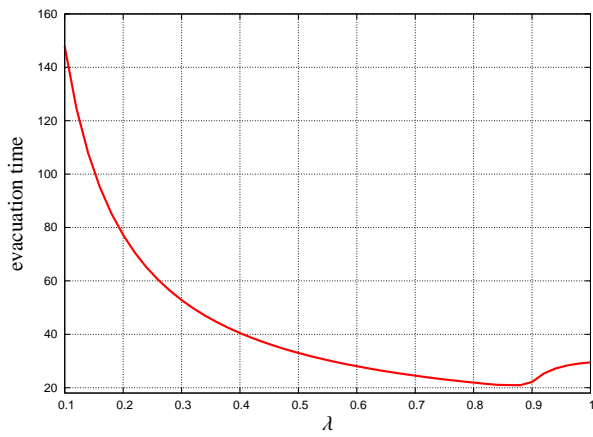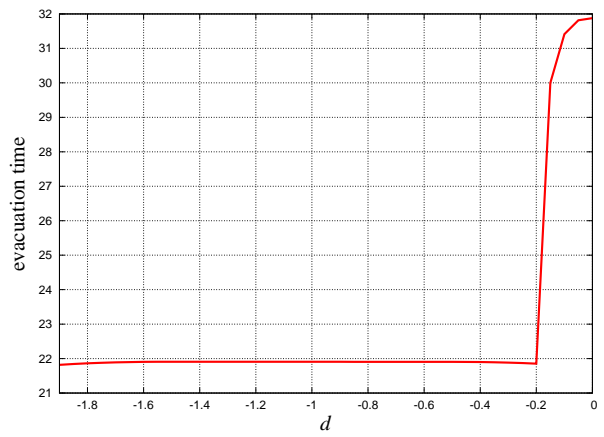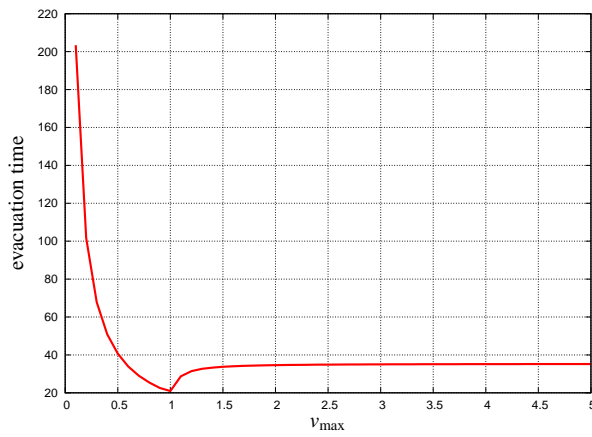
Figure 10: With reference to Subsection 4.2: Braess paradox simulations: density profiles at times $t = 1$ (first line), $t = 7$ (second line), $t = 15$ (third line), $t = 19$ (fourth line) and $t = 24.246$ (last line).

(a) Evacuation time as a function of λ.

(b) Evacuation time as a function of d.

(c) Evacuation time as a function of $v_{\max}$.

Figure 11: With reference to Subsection 4.3: Evacuation time as a function of different parameters of the model.
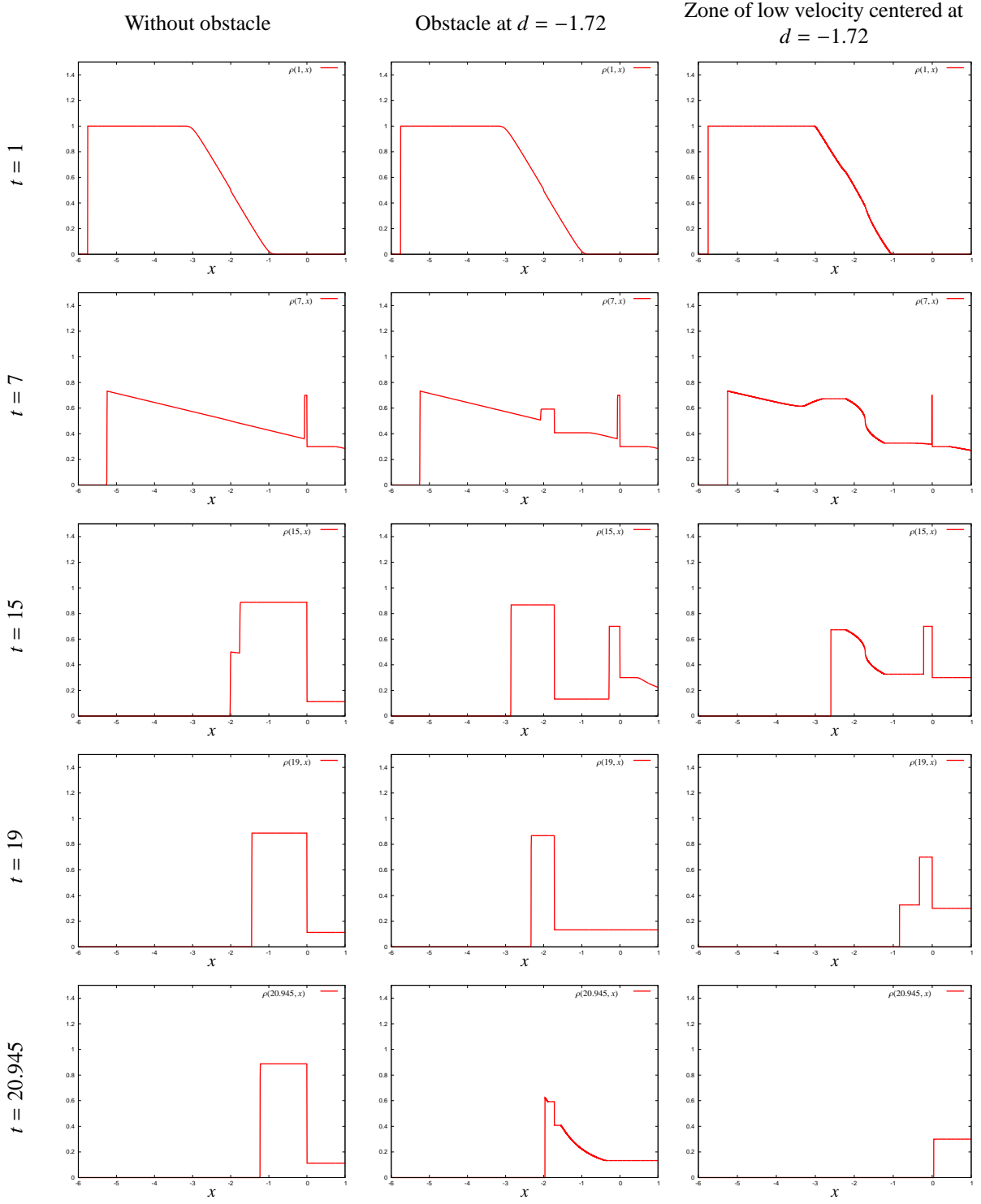
15

Figure 12: With reference to Subsection 4.3: Braess' paradox and zone of low velocity simulations: density profiles at times $t = 1$ (first line), $t = 7$ (second line), $t = 15$ (third line), $t = 19$ (fourth line) and $t = 20.945$ (last line).

[18] B. Andreianov, C. Donadello, U. Razafison, M. D. Rosini, Riemann problems with non–local point constraints and capacity drop, Mathematical Biosciences and Engineering 12 (2) (2015) 259–278. doi:10.3934/mbe.2015.12.259.

[19] R. M. Colombo, P. Goatin, A well posed conservation law with a variable unilateral constraint, J. Differential Equations 234 (2) (2007) 654–675. doi:10.1016/j.jde.2006.10.014.
URL http://dx.doi.org/10.1016/j.jde.2006.10.014

[20] C. Chalons, P. Goatin, N. Seguin, General constrained conservation laws. Application to pedestrian flow modeling, Netw. Heterog. Media 8 (2) (2013) 433–463. doi:10.3934/nhm.2013.8.433.
URL http://dx.doi.org/10.3934/nhm.2013.8.433

[21] S. Kružhkov, First order quasilinear equations with several independent variables., Mat. Sb. (N.S.) 81 (123) (1970) 228–255.

[22] E. Godlewski, P.-A. Raviart, Numerical approximation of hyperbolic systems of conservation laws, Vol. 118 of Applied Mathematical Sciences, Springer-Verlag, New York, 1996. doi:10.1007/978-1-4612-0713-9.
URL http://dx.doi.org/10.1007/978-1-4612-0713-9

[23] R. J. LeVeque, Finite volume methods for hyperbolic problems, Cambridge Texts in Applied Mathematics, Cambridge University Press, Cambridge, 2002. doi:10.1017/CBO9780511791253.

[24] D. Parisi, C. Dorso, Microscopic dynamics of pedestrian evacuation, Physica A: Statistical Mechanics and its Applications 354 (0) (2005) 606 – 618. doi:http://dx.doi.org/10.1016/j.physa.2005.02.040.

[25] A. Aw, M. Rascle, Resurrection of "second order" models of traffic flow, SIAM J. Appl. Math. 60 (3) (2000) 916–938 (electronic). doi:10.1137/S0036139997332099.

[26] H. Zhang, A non-equilibrium traffic model devoid of gas-like behavior, Transportation Research Part B: Methodological 36 (3) (2002) 275 – 290. doi:http://dx.doi.org/10.1016/S0191-2615(00)00050-3.

[27] R. M. Colombo, G. Facchi, G.and Maternini, M. D. Rosini, On the continuum modeling of crowds, in: Hyperbolic problems: theory, numerics and applications, Vol. 67 of Proc. Sympos. Appl. Math., Amer. Math. Soc., Providence, RI, 2009, pp. 517–526. doi:10.1090/psapm/067.2/2605247.

[28] R. Colombo, P. Goatin, M. Rosini, On the modelling and management of traffic, ESAIM: Mathematical Modelling and Numerical Analysis 45 (05) (2011) 853–872. doi:10.1051/m2an/2010105.